MODELLING OF DIRECT CONTACT CONDENSATION IN HORIZONTALLY STRATIFIED FLOW WITH CFX CODE

Luka Štrubelj
Jožef Stefan Institute
Reactor Engineering Division
Jamova 39, SI-1000,
Ljubljana, Slovenia
Phone: 00386 588 5312
Fax: 00386 588 5377
luka.strubelj@ijs.si

Iztok Tiselj
Jožef Stefan Institute
Reactor Engineering Division
Jamova 39, SI-1000,
Ljubljana, Slovenia
Phone: 00386 588 5330
Fax: 00386 588 5377
iztok.tiselj@ijs.si

Boštjan Končar
Jožef Stefan Institute
Reactor Engineering Division
Jamova 39, SI-1000,
Ljubljana, Slovenia
Phone: 00386 588 5260
Fax: 00386 588 5377
bostjan.koncar@ijs.si

Abstract

Direct contact condensation and condensation induced water-hammer in a horizontal pipe was experimentally investigated at PMK-2 test facility of the Hungarian Atomic Energy Research Institute KFKI. The experiment is preformed in the horizontal section of the steam line of the PMK-2 integral test facility. As liquid water floods the horizontal part of the pipeline, the counter current horizontally stratified flow is being observed. During the flooding of the steam line, the vapour-liquid interface area increases and therefore the vapour condensation rate and the vapour velocity also increase. In this paper simulation of the experiment with thermal phase change model based on surface renewal concept with small eddies for calculation of heat transfer coefficient.

Introduction

Only a limited analytical approach to the problem of Direct Contact Condensation (DCC) in horizontal stratified flow is possible, therefore experiments are necessary. Two frequently used correlations for heat and mass transfer during the DCC in stratified flow were derived from experimental results by Lim et.al. [24] and Kim, Lee and Bankoff [20]. Unlike Lim et. al. [24] and Kim et .al. [20] who performed their experiments in a pipe, Celata et. al. [8] measured DCC on a slowly moving subcooled water in a "pressurizer-like" geometry and developed a special set of correlations for that purpose. Chan and Yuen [10] used the experimental device of Lim et. al. [24] and analyzed the influence of air on the DCC in stratified horizontal flow.

Hughes and Duffey [17] introduced a "surface renewal theory" for DCC in turbulent separated flow, which points to an important role of the turbulence in the liquid layer. Experiments and models of DCC in a rectangular duct and rectangular tank were later described by Lorencez et. al. [26] and Mikielewicz et. al. [28], respectively. Especially Lorencez et. al. [26] with their sophisticated experiment made a detailed measurement of the turbulence near the free surface and clarified the impact of the turbulence on the interfacial heat and mass transfer coefficients. Chun, Yu [13] described their air-water and steam-water experiments in nearly horizontal stratified flow and compared various correlations for the stratified-to-slug transition with their experiments. They suggested a new model, which gives (comparing to Mishima and Ishii [29], and Taitel and Dukler [41]) more accurate prediction of transition at low liquid superficial velocities. Ramamurti et. al. [36] performed a DCC experiment on a thick layer of moving water in the vessel with a stagnant vapour bubble and expressed the heat transfer coefficients in terms of Nusselt number as a function of liquid Reynolds and Prandtl number and the sub-cooling intensity. The recent paper of Kim, Park, Song [21] is about DCC in a steam plume, however it deserves to be mentioned due to the clear literature overview of the DCC in the horizontally stratified flow.

One of the most important phenomena in the nuclear thermal-hydraulics is behavior of the cold Emergency Core Cooling (ECC) water injected from the top or from the bottom into the horizontal section of the hot leg near the reactor vessel during the loss of coolant accident (Kircher and Bankoff [22]). Ohnuki et. al. [31] analyzed the influence of the scale (pipe diameter) on the stratified flow during the ECC injection into the stratified flow in the hot leg from the bottom side. They compared their own experimental results obtained on a small scale and results obtained on full scale UPTF device (Mayinger et. al. [27]). Aya and Nariai [4] examined the past experimental DCC data and focused on the phenomena appearing during the ECC injection from the top side of the hot leg where DCC appears also on the cold liquid jet and not only in the horizontally stratified flow regime. Another experimental study where ECC is injected from the top of the hot leg of the COSI experimental device is described by Janicot and Bestion [19]. Today, the issues of ECC injection are still relevant for nuclear safety - for example - Gargallo et. al. [15] used a new test facility WENKA and developed a new counter-current flow limitations criterion during the hot leg injection.

DCC models in 1D two-fluid computer codes

Most of the DCC models described in the previous section were later tested in 1D computer codes for simulations of the various thermal-hydraulic fast transients, mainly in the field of nuclear engineering. Ohnuki et. al. [32] has focused on the interfacial friction model around the Counter-Current Flow Limit (CCFL) in gas liquid flow and built and tested their model in the TRAC code. Asaka et. al. [3] improved the interfacial drag model in TRAC [44] in high-pressure horizontally stratified flow. Zhang et. al. [50] tested and compared Lim's [24] and Bankoff's [20] correlations in TRAC. Janicot and Bestion [19] applied the results of the COSI experiment on ECC condensation measurements and improved the DCC correlations in stratified flow in CATHARE (Bestion [6]). Choi et. al. [11] improved RELAP5 correlations for DCC in horizontally stratified flow [7] by taking into account the presence of the non-condensable gas and it's influence on the condensation rate. Similar

work was performed by Park et. al. [33] who modified RELAP5/MOD3 with new correlations for DCC in horizontal (and vertical) stratified flows.

Condensation induced water hammer (CIWH) in horizontal pipes

CIWH in horizontal pipes is a safety issue for various fields of engineering. The phenomenon starts with DCC of steam on subcooled liquid in horizontally stratified flow. Once the slug is formed, a rapid condensation of the bubble entrapped behind the slug may follow, resulting in a strong pressure peak. Most of the CIWH studies are related with the nuclear energy, however, the phenomenon is relevant also for other fields (see Streicher [39] , CIWH in solar thermal plants).

Chun and Yu [12] developed a set of prevention guidelines based on analytical approximations and their experimental research of condensation-induced water hammer. Yao et. al. [49] and He et. al. [16] presented their CIWH experiment in a horizontal pipe and 2D numerical simulations of the phenomena with a VOF model for interfacial tracking, however, their results were obtained on very coarse grids. Ansari [2] presented his own experimental device for CIWH in horizontally stratified flow and suggested a correction to the Mishima, Ishii [29] model for stratified-to-slug transition. Another set of experiments with improved vapour volume fraction measurement was run at Hungarian KFKI experimental device PMK2 (Prasser et. al. [34] and [35]) within the WAHALoads project of the 5th EU research program. Attempts to describe the KFKI experiment with the 1D two-fluid model of the WAHA code (Tiselj et. al. [43]) pointed to large uncertainties of the simulations related to the model of stratified-to-slug flow transition and correlations for interfacial heat, mass and momentum transfer.

CFD and DCC in horizontally stratified flow

Various techniques for multidimensional simulations of stratified flows are described in the literature. Several review papers can be found in "Annual review of Fluid Mechanics": Tsai and Yue [45] discuss computation of free-surface flows with interface tracking algorithms mainly from the standpoint of maritime and ocean engineering. They present boundary-discretization methods applicable for potential free surface flows and volume-discretization methods for the flows that are not irrotational. Among the volume-discretization methods, which are considered to be relevant for the modeling of the DCC, the most important techniques for the interface tracking (IT) are probably: VOF method reviewed by Scardovelli and Zaleski [37], level-set method reviewed by Sethian and Smereka [38], and the method of Unverdi and Tryggvason [46]. All these methods consider the interface as a physical discontinuity, although Unverdi and Tryggvason [46] applied a numerically diffuse description of the interface. The assumption of the sharp-interface is not always appropriate (Anderson et. al., [1]) as the thickness of the interface may not be negligible comparing to the relevant scales especially near the critical temperature. Anderson et. al. [1] present a review of the models and methods, that can be applied for simulations of diffuse-interfaces of finite thickness. An innovative approach by Lakehal et. al. [23] based on pseudo-spectral DNS of turbulent wavy flow at low Reynolds number is to be mentioned, as a very accurate tool, but like all today's DNS studies - limited to a narrow range of flows. Another option for multidimensional simulations of two-phase flows is a two-fluid model, which can be found mainly in 1D nuclear thermal-hydraulic codes. However, the multidimensional two-fluid models with suitable algorithms for tracking of the "major" interfaces, might be an alternative to the pure interface tracking methods, which fail when the surface characteristic scales become comparable or smaller than the grid size (see Yadigaroglu, [47] , for discussion about two-fluid and interface tracking models of two-phase flow). An example of such two-fluid model is used in CFD code CFX5, which was used by Mouza et. al. [30] for simulation of the 3D wavy stratified flow without condensation on ~60000 grid points. Berthelsen and Ytrehus [5] performed 2D simulation of stratified flow in a pipe without condensation, assuming steady-state turbulent flow without condensation. A further example of multidimensional two-fluid model for

stratified flow can be found in a paper by Line and Lopez [25], where only 1D results for wavy stratified flow are shown. Simulations of stratified flow with a 2D two-fluid model are further performed by Yao et. al. [48], who made simulations of stratified flow with and without the condensation. 2D CFD simulations of ECC injection of subcooled water into horizontally stratified hot leg flow were performed by Coste [14] using two-fluid model with interfacial heat and mass transfer model based on surface renewal concept.

Experiment

Test section of the water hammer facility is shown in figure 1 and consists of a 2.87 m long horizontal pipe with inner diameter 73 mm (No. 1 in fig. 1). Steam generator (SG head - No. 4 in fig. 1) supplies vapour for the test section through the vapour inlet head (No. 2) which extends the horizontal test section for 0.2 m and serves as a 90 degree bend and as an inertia block (mass 200 kg). Liquid inlet head (No. 3) geometry is similar to the vapour inlet head, distance between the centers of both inlet heads is 3.20 m. Steam-line section (No. 5) connected to the condenser (not shown in fig. 1) is isolated in the water hammer experiment. The supply of cold water is obtained with a 75 liter water tank (No. 6 in fig. 1) pressurized with nitrogen and connected to the bottom of the vertical steam-line section below the liquid inlet head (No. 3). Water is injected by opening the valve (No. 11 in fig 1) in the injection line (inner diameter 24 mm).

All together, 35 water hammer experiments at the PMK-2 device were performed, at initial steam pressures between 10 and 40 bar and at tank water temperatures between 17 and 140 ^{0}C. Cold water mass flow rates were between 0.7 and 1.7 kg/s. Before the start of each experiment the whole construction was heated with steam for a few hours. Steam pressure in the pipe and water tank flow rate can be considered as constant during the transient.

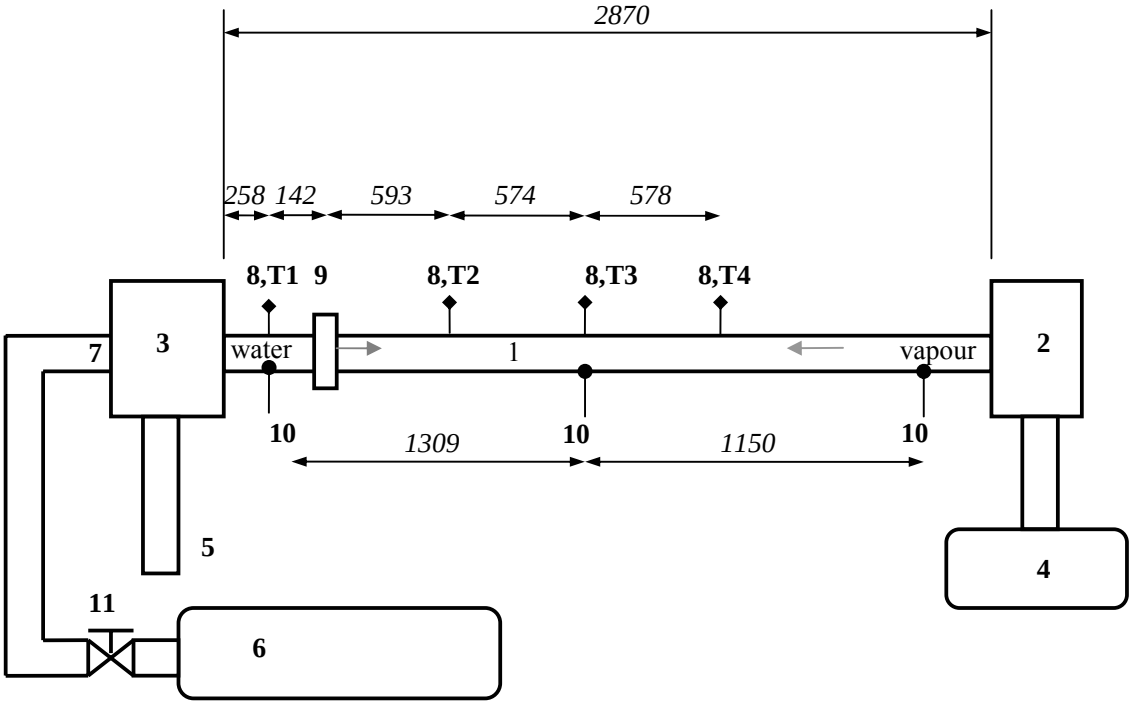

Figure 1: Water hammer test section at the PMK-2 facility.

Instrumentation

The following instrumentation was used in the experiment:

- Wire-mesh sensor (No. 9 in fig. 1) measures cross-sectional distribution of vapour volume fraction and cross sectional temperature field.
- Four local void probes with integrated thermocouple (No. 8 in fig. 1).
- Three pressure transducers (No. 10 in fig. 1,).
- Two displacement cells - strain gauges (No. 7 in fig. 1) measuring axial and radial strain behind the vapour and liquid inlet heads.

Experimental results

There were 35 water hammer experiments performed at PMK-2 and described in the reports by Prasser et. al, [34] and [35]. The most important results for this paper are actually a mesh sensor vapour volume fraction and temperature profile measurements, and not the water hammer pressure peaks. Mesh sensor data are the most important for the development and verification of the heat and mass transfer models in a horizontally stratified flow, which are responsible for the instability onset. Magnitude of the water hammer pressure peak is less important for the work planned within the NURESIM project.

It is important to stress rather the large uncertainty of the experiments - especially the maximum pressure peaks recorded: two experiments performed at very similar initial conditions can give very different pressure peaks with a difference of factor ~2 not uncommon.

Simulation

CFX-5.7 was used for simulation of experiment. The domain was discretized with a structured grid. More about models and numerical methods can be found in CFX documentation [9]. Initial and boundary conditions are the same as in the experiment and can be seen in figure 2.

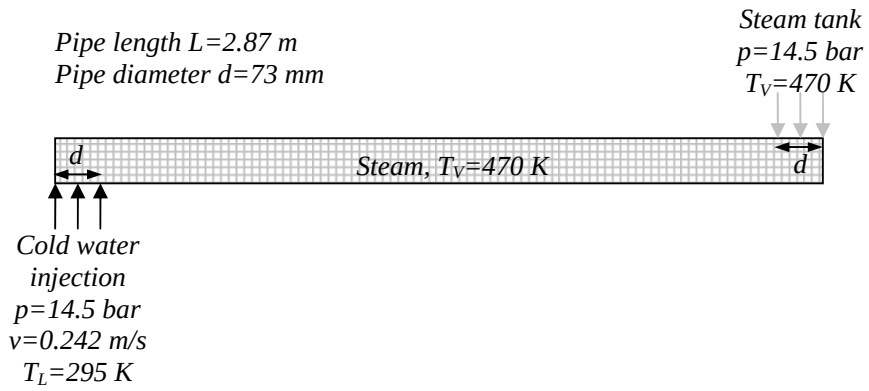

Figure 2: Initial and boundary condition.

Continuity equation for liquid and was solved

$$\frac{\partial}{\partial t}(\alpha\rho_L)+\nabla\cdot(\alpha\rho_L\vec{U})=\Gamma, \tag{1}$$

where t denotes time, α - liquid volume fraction, ρ_L – liquid density, $\vec{U}$ - velocity field and Γ - mass source per unit volume. Volume fraction of steam can be expressed as 1-α and continuity equation for vapour as

$$\frac{\partial}{\partial t}\left((1-\alpha)\rho_V\right)+\nabla\cdot\left((1-\alpha)\rho_V\vec{U}\right)=-\Gamma\,, \tag{2}$$

where ρ_V stands for vapour density. Homogeneous momentum model was used

$$\frac{\partial}{\partial t}\left(\rho\vec{U}\right)+\nabla\cdot\left(\rho\vec{U}\otimes\vec{U}-\mu_{eff}\left(\nabla\vec{U}+\left(\nabla\vec{U}\right)^T\right)\right)=-\nabla p'\,, \tag{3}$$

where $\mu_{eff}=\mu+\mu_t$ stands for effective viscosity, $\mu_t=C_\mu\rho\frac{k^2}{\varepsilon}$ for turbulent viscosity, constant $C_\mu=0.09$ and $p'=p+\frac{2}{3}\rho k$ for modified pressure. Density is calculated as $\rho=\alpha\rho_L+(1-\alpha)\rho_V$ and viscosity as $\mu=\alpha\mu_L+(1-\alpha)\mu_V$. We used the k-ε turbulent model for a homogeneous mixture

$$\frac{\partial}{\partial t}\left(\rho k\right)+\nabla\cdot\left(\rho\vec{U}k\right)=\nabla\cdot\left(\left(\mu+\frac{\mu_t}{\sigma_k}\right)\nabla k\right)+P_k-\rho\varepsilon\,, \tag{4}$$

$$\frac{\partial}{\partial t}\left(\rho\varepsilon\right)+\nabla\cdot\left(\rho\vec{U}\varepsilon\right)=\nabla\cdot\left(\left(\mu+\frac{\mu_t}{\sigma_\varepsilon}\right)\nabla\varepsilon\right)+\frac{\varepsilon}{k}\left(C_{\varepsilon1}P_k-C_{\varepsilon2}\rho\varepsilon\right), \tag{5}$$

where ε denotes turbulent eddy dissipation, k - turbulence kinetic energy, constants are $C_{\varepsilon1}=1.44$, $C_{\varepsilon2}=1.92$, $\sigma_\varepsilon=1.3$, $\sigma_k=1.0$ and P_K is turbulent production due to viscosity

$$P_k=\mu_t\nabla\vec{U}\cdot\left(\nabla\vec{U}+\nabla\vec{U}^T\right)-\frac{2}{3}\nabla\cdot\vec{U}\left(3\mu_t\nabla\cdot\vec{U}+\rho k\right). \tag{6}$$

Separate energy equations for liquid and steam were modeled

$$\begin{aligned}\frac{\partial}{\partial t}\left(\rho h_{L,tot}\right)-\alpha\frac{\partial p}{\partial t}+\nabla\cdot\left(\rho\vec{U}h_{L,tot}-\alpha\lambda_L\nabla T_L\right)-\nabla\cdot\left(\alpha\mu_L\left(\nabla\vec{U}+\left(\nabla\vec{U}\right)^T-\frac{2}{3}\nabla\vec{U}\delta\right)\vec{U}\right)=\\ \Gamma\left(h_{V,tot}-h_{L,tot}\right)+HTC_L A\left(T_V-T_L\right),\end{aligned} \tag{7}$$

$$\begin{aligned}\frac{\partial}{\partial t}\left(\rho h_{V,tot}\right)-(1-\alpha)\frac{\partial p}{\partial t}+\nabla\cdot\left(\rho\vec{U}h_{V,tot}-(1-\alpha)\lambda_V\nabla T_V\right)-\nabla\cdot\left((1-\alpha)\mu_V\left(\nabla\vec{U}+\left(\nabla\vec{U}\right)^T-\frac{2}{3}\nabla\vec{U}\delta\right)\vec{U}\right)=\\ -\Gamma\left(h_{V,tot}-h_{L,tot}\right)-HTC_L A\left(T_V-T_L\right),\end{aligned} \tag{8}$$

where λ denotes thermal conductivity, T – temperature, $h_{tot}=h_{stat}+\frac{1}{2}\left(\vec{U}\cdot\vec{U}\right)$ - total specific enthalpy and h_{stat} - static specific enthalpy. The interphase mass source per unit volume is calculated as $\Gamma=\dot{m}A$, where interphase area density is $A=\left|\nabla\alpha\right|$. Interphase mass flow rate per unit interfacial area is calculated as

$$\dot{m}=\frac{HTC_L\left(T_{sat}-T_L\right)}{h_{V,sat}-h_L}, \tag{9}$$

where HTC_L stands for liquid heat transfer coefficient and $T_{sat}=T_{sat}(p)$ for saturation temperature. The heat transfer coefficient is calculated using surface renewal theory introduced by Hughes and Duffey [17]:

$$HTC_L=2\rho_L c_{p,L}\left(\frac{a_L}{\pi}\right)^{1/2}\left(\frac{\varepsilon}{\mu_L/\rho_L}\right)^{1/4}, \tag{10}$$

where $a_L=\frac{\lambda_L}{\rho_L c_{p,L}}$ is thermal diffusivity. Liquid and vapour are modeled as a compressible and temperature dependent phases using Real Gas Properties (RGP) table which contains specific enthalpy *h(T,p)*, speed of sound *s(T,p)*, specific volume *v(T,p)*, specific heat at constant volume c_v*(T,p)*, specific heat at constant pressure c_p*(T,p)*, $(\partial p/\partial v)_T$, specific entropy *s(T,p)*, dynamic viscosity $\mu=\mu$ *(T,p)* and

thermal conductivity $\lambda(T,p)$. The table was created using 500 non-equi-pressure-distant points and 500 equi-temperature-distant points from the triple point (611 Pa, 273.15 K) to critical water point (220.55 bar, 647 K).

Results

Surface evolution, interfacial mass transfer rate and heat transfer coefficient were observed during the transient (see fig. 3). The pictures are not in real aspect ratio (2.87 m : 73 mm). The first assumption was that the Kelvin-Helmholtz instability (Thorpe [42], simulated by Štrubelj and Tiselj [40]) is the mechanism that leads to the slug appearance and rapid condensation of the bubble entrapment by the slug. From CFD simulation (see fig. 3) it is seen that reflection of the wave (at 4.5 s) is the mechanism that leads to bubble entraption (at 7.5 s), but no water hammer is observed (timestep was small enough to track pressure waves in water $\Delta t = \Delta x / c = 4 \cdot 10^{-6}$ s). In experiment [34] and [35] and WAHA code [18] simulation water hammer is observed. The most intensive condensation is around the wave reflected from the right side of the pipe. The interface mass transfer rate is up to 10 kg/m^{3}s, and heat transfer coefficient is up to 200,000 W/m^{2}K. The pipe is full of water in approximately 18 s. The mass of condensed vapour in 10 s is 0.15 kg, which is 175% of horizontal section volume, or 1.3 % of whole water mass (pipe full of water).

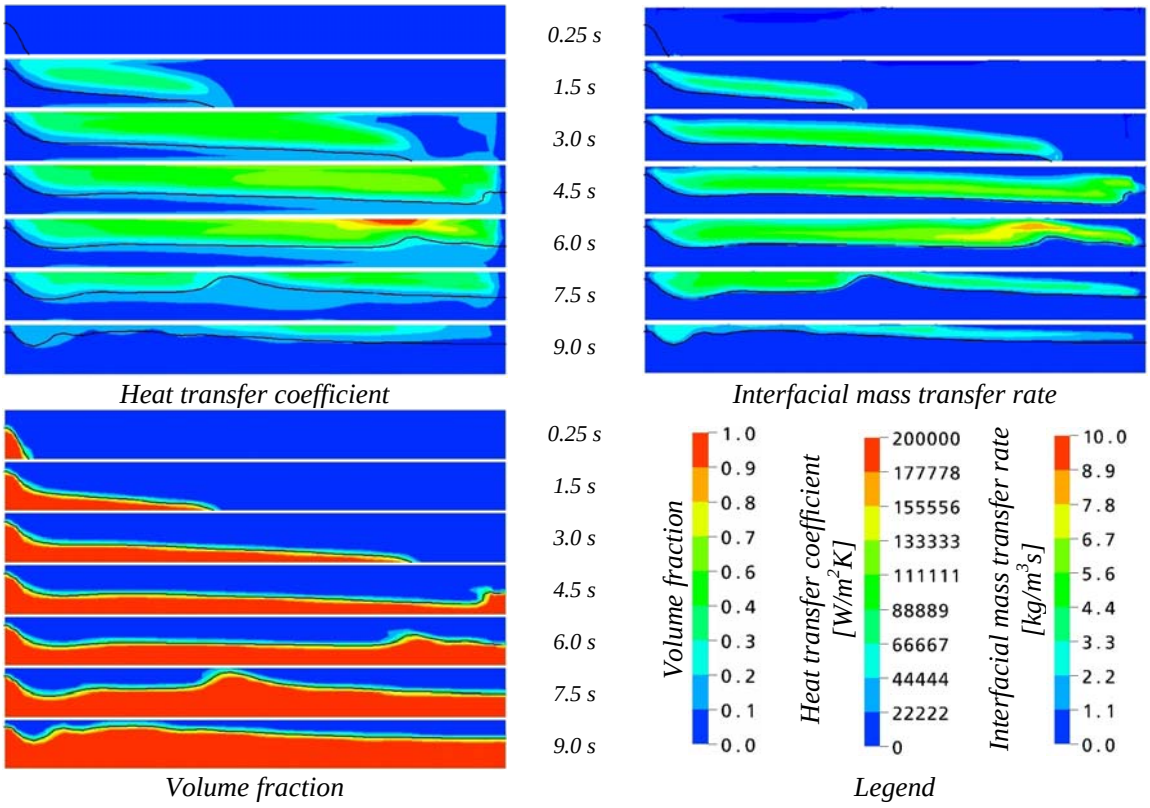

Figure 3: 2D simulation.

The condensation rate [kg/s] versus time is plotted in figure 4 using different number of volumes in pipe diameter (2D), different time steps (Courant-Friedrich-Levy number CFL=$\Delta t/(\Delta x \cdot u_{inlet})$) on 10x400 volumes and different mesh edge ratios. These parameters have no significant influence on the condensation rate. Comparison with 3-dimensional simulation (4500 volumes, 10 volumes in

diameter) is done. The channel in the 2D simulation has the same pipe cross-section as in 3D. The 3D effect is not very important (see fig 4).

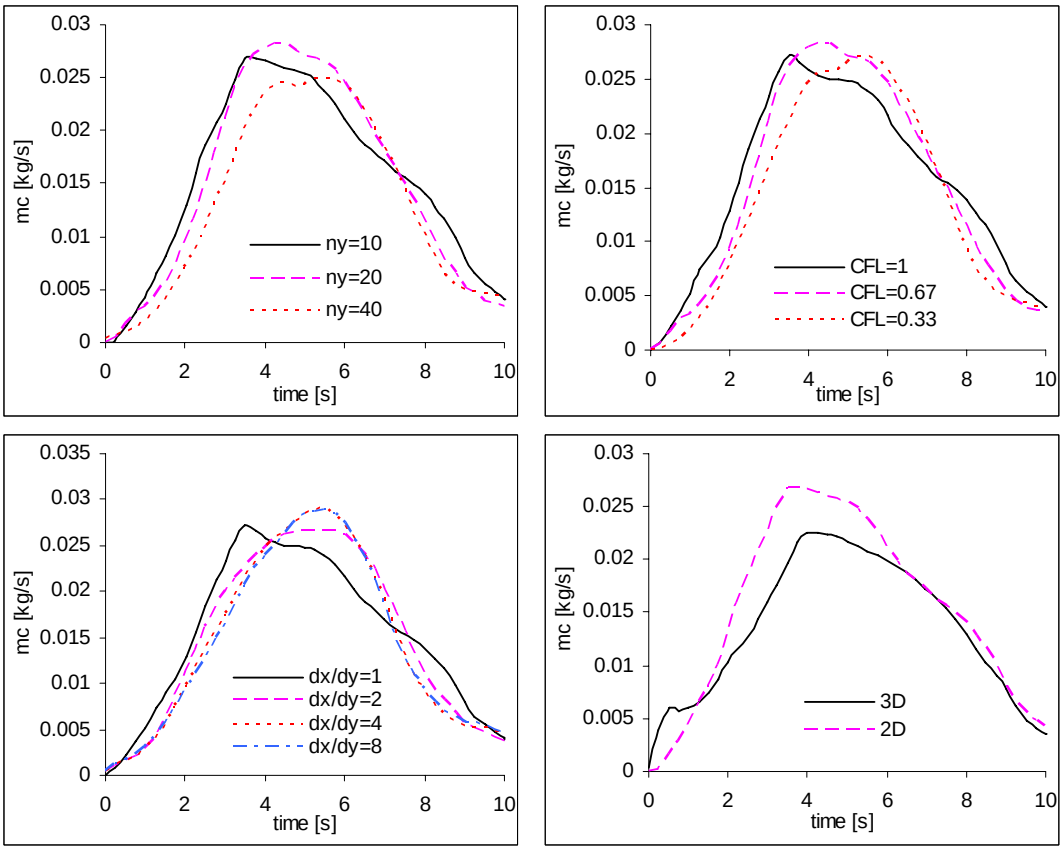

Figure 4: Interfacial mass transfer rate (mc) using different grid spacing (upper left), different timestep (upper right), different mesh edge length ratio (lower left) and comparison between 2D and 3D simulation.

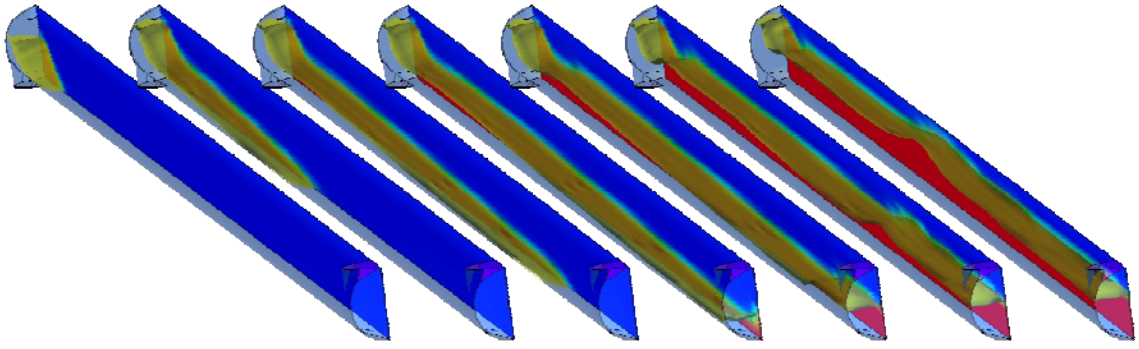

Figure 5: 3D simulation, izosurface (volume fraction=0.5) at 0.25, 1.5, 3, 4.5, 6, 7.5 and 9 s.

Local vapour volume fractions and temperatures in the simulation are compared with measurements (see fig. 6). In the experiment local measurements are at 4 different locations (see fig. 1). Temperature of the water in simulation is only slightly increased (upper right picture in fig. 6), in experiment this temperature is increased much more (lower right picture in fig. 6). Smaller steam

condensation rate may be the reason for this. From measurement of water and steam inflow the condensation rate could be calculated. To estimate propagation of water at the bottom of the pipe, measurement should take place at the bottom of the pipe. The measurement begins when the valve (no 11 in fig. 1) is opened. The cold water needs some time to get into the test section from the valve, which can be estimated, but additional volume fraction sensor at beginning of test section eliminates the error from estimation of this time.

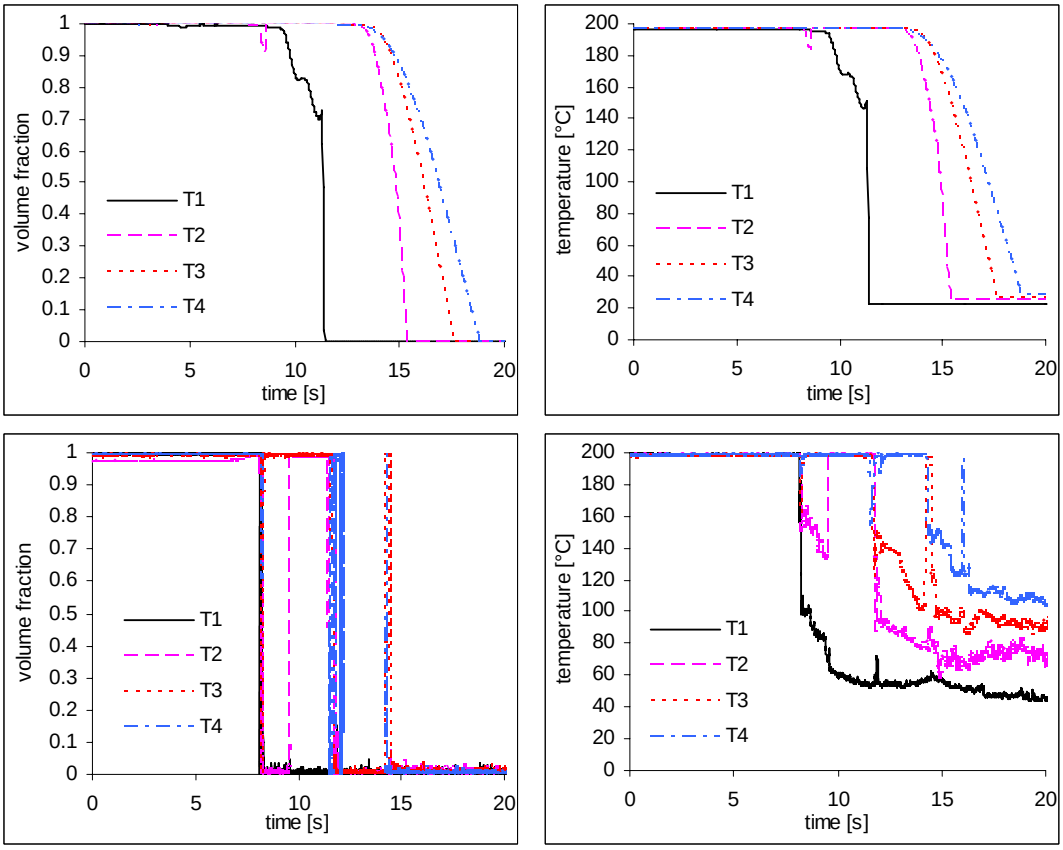

Figure 6: Volume fraction in simulation (upper left) and in experiment (lower left); temperature in simulation (upper right) and in experiment (lower right) at 4 different locations.

The wire-mesh sensor has 12 electrode rods vertically positioned at the center of the pipe, from which water level can be measured with *D*/12 accuracy. Real value of water level is between two lines (green and red) in figure 7. At the beginning of the experiment we have water at the bottom of the pipe, which comes from wall condensing vapour, but only an estimate from the wire mesh sensor is available (was not taken into account in simulation). In the simulation water level at the wire-mesh sensor position increases from zero when water partially floods the wire-mesh sensor, and second significant increase is due to reflection wave from right end of pipe. In experiment flooding of wire-mesh sensor occurs later than in simulation (see fig. 7).

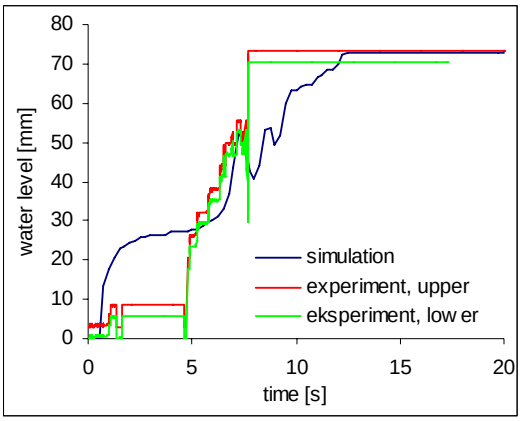

Figure 7: Water level in pipe; comparison between simulation and experimental measurement, which is between lower (green) and upper value (red).

Conclusions

With surface renewal theory condensation rate and mass of condensed vapour is lower than in experiment. This is visible from small water temperature increase. Condensation rate is not significantly dependent on the timestep and mesh size. No water hammer is observed in the simulation, but entrapment of a bubble due to refraction wave from the end of a pipe is clearly visible. In the next set of experiments additional measurements were proposed: steam inflow (to calculate of condensation rate), local measurement of void and temperature at the bottom of the pipe (propagation of water at the bottom) and an additional mesh-sensor (to measure velocity of refraction wave); which makes comparison with simulation more complete.

References

[1] Anderson D. M., McFadden G. B., Wheeler A. A., 1998. Diffuse-interface methods in fluid mechanics. *Annual Review of Fluid Mechanics*, **30**, 139–65.

[2] Ansari M. R., 1999. Slug induced water-hammer in steam-water stratified two-phase flow during condensation phenomena. *Proceedings of 3rd ASME/JSME Joint Fluids Engineering Conference*, FEDSM99-6893, San Francisco, CA.

[3] Asaka H., Kukita Y., Anoda Y., Nakamura H., Tasaka K., 1991. Improvement of TRAC-PF1 interfacial drag model for analysis of High-Pressure Horizontally-Stratified two-phase flow. *Journal of Nuclear Science and Technology* **28** (1) 33-44.

[4] Aya I., Nariai H., 1991. Evaluation of heat-transfer coefficient at direct contact condensation of cold water and steam. *Nuclear Engineering and Design* **131**, 17-24.

[5] Berthelsen P.A., Ytrehus T., 2005, Calculations of stratified wavy two-phase flow in pipes. *International Journal of Multiphase flow* **31** (5), 571-592.

[6] Bestion D., 1990 . The physical closure laws in the cathare code, *Nuclear Engineering and Design*, **124**, 229-245.

[7] Carlson K. E., Riemke R. A., Rouhani S. Z., Shumway R. W., and Weaver W. L., 1990, RELAP5/MOD3 Code Manual, Vols. 1–7, NUREG/CR-5535, EG&G Idaho, Idaho Falls.

[8] Celata G. P., Cumo M., Farello G. E.,Focardi G., 1986. Direct contact condensation of steam on slowly moving water. *Nuclear Engineering and Design* **96**, 21-31.

[9] CFX-5.7.1 Documentation, Solver Theory, Multiphase Flow Theory, ANSYS, 2005.

[10] Chan T.S. , Yuen M. C., 1990. The effect of air on condensation of stratified horizontal concurrent steam water-flow. *Journal of heat transfer - T ASME* **112** (4), 1092-1095.

[11] Choi K. Y., Chung H. J., No H. C., 2002. Direct-contact condensation heat transfer model in RELAP5/MOD3.2 with/without noncondensable gases for horizontally stratified flow. *Nuclear Engineering and Design* **221**,139-151.
[12] Chun M.-H., Yu S.-O., 2000. A parametric study and a guide chart to avoid condensation-induced water hammer in a horizontal pipe. *Nuclear Engineering and Design* **201**, 239-257.
[13] Chun M.-H., Yu S.-O., 2000. Effect of steam condensation on countercurrent flow limiting in nearly horizontal two-phase flow. *Nuclear Engineering and Design* **196**, 201-217.
[14] Coste P., 2004. Computational simulation of multi-D liquid –vapour thermal shock with condensation. *5th International Conference on Multiphase Flow (ICMF'04)*, paper no. 420.
[15] Gargallo M., Schulenberg T., Meyer L., Laurien E., 2005. Counter-current flow limitations during hot leg injection in pressurized water reactors. *Nuclear Engineering and Design* **235**, 785-804.
[16] He F., Yang J., Wang X., 2000. Condensation-induced steam bubble collapse in a pipeline. *Tsinghua science and technology* **5**, 424-427.
[17] Hughes E. D., Duffey R. B., 1991. Direct contact condensation and momentum-transfer in turbulent separated flows. *International Journal of Multiphase flow* **17** (5), 599-619.
[18] J. Gale, I. Tiselj, I. Parzer, Modelling of condensationinduced water hammer, *Proc. of the 3rd International Symposium on Two-Phase Flow Modelling and Experimentation*, 2004.
[19] Janicot A., Bestion D., 1993. Condensation modelling for ECC injection. *Nuclear Engineering and Design* **145**, 37-45.
[20] Kim H. J., Lee S. C., Bankoff S. G., 1985. Heat transfer and interfacial drag in countercurrent steam-water stratified flow. *International Journal of Multiphase Flow* **11** (5), 593-606.
[21] Kim Y.-S., Park J.-W., Song C.-H, 2004. Investigation of the steam-water direct contact condensation heat transfer coefficients using interfacial transport models. *International Communications in Heat and Mass Transfer* **31**, 397-408.
[22] Kirchner W., Bankoff S. G., 1985. Condensation effects in reactor transients. *Nuclear Science and Engineering* **89**, 310-321.
[23] Lakehal D, Fulgosi M, Yadigaroglu G, Banerjee S, 2003. Direct numerical simulation of turbulent heat transfer across a mobile, sheared gas-liquid interface. *Journal of heat transfer - T ASME* **125** (6), 1129-1139.
[24] Lim I. S., Tankin R. S., Yuen M. C., 1984, Condensation measurement of horizontal cocurrent steam-water flow. *Journal of Heat Transfer - T ASME* **106**, 425-432.
[25] Line A., Lopez D., 1997. Two-fluid model of wavy separated two-phase flow. *International Journal of Multiphase flow* **23** (6), 1131-1146.
[26] Lorencez C., Nasr-Esfahany, Kawaji M., 1997. Turbulence structure and prediction of interfacial heat and mass transfer in wavy-stratified flow. *AIChE Journal* **43**, 1426-1435.
[27] Mayinger F, Weiss P, Wolfert K, 1993. 2-phase flow phenomena in full-scale reactor geometry. *Nuclear Science and Engineering* **145**, 47-61.
[28] Mikielewicz J., Trela M., Ihnatowicz E., 1997. A theoretical and experimental investigation of dorect contact condensation on a liquid layer. *Experimental Thermal and fluid Science* **15**, 221-227.
[29] Mishima K, Ishii M., 1980. Theoretical prediction of onset of horizontal slug flow. *Journal of Fluids Engineering-T ASME* **102** (4), 441-445.
[30] Mouza A. A., Paras S. V., Karabelas A. J., 2001. CFD code application to wavy stratified gas-liquid flow. *Chemical Engineering Research and Design* **79**(A5), 561-568.
[31] Ohnuki A., Adachi H., Murao Y., 1988. Scale effects on countercurrent gas-liquid flow in a horizontal tube connected to inclined riser. *Nuclear Engineering and Design* **107**, 183-294.
[32] Ohnuki A., Akimoto H., Murao Y., 1992. development of interfacial friction model for two-fluid model code against countercurrent gas-liquid flow limitation in PWR hot leg. *Journal of Nuclear Science and Technology* **29** (3), 223-232.
[33] Park H. S., No H. C., Bang Y. S., 2003. Analysis of experiments for in-tube steam condensation in the presence of noncondensable gases at a low pressure using the RELAP5/MOD3.2 code

modified with a non-iterative condensation model. *Nuclear Engineering and Design* **225** (2-3), 173-190.
[34] Prasser H. M., Ezsol G., Baranyai G., 2004. PMK-2 water hammer tests, condensation caused by cold water injection into main steam-line of VVER-440-type PWR - Quick-Look Report (QLR), *WAHALoads project deliverable D48*.
[35] Prasser H. M., Ezsol G., Baranyai G., 2004. PMK-2 water hammer tests, condensation caused by cold water injection into main steam-line of VVER-440-type PWR - Data Evaluation Report (DER), *WAHALoads project deliverable D51*.
[36] Ramamurthi K, Kumar Sunil S., 2001. Collapse of vapour locks by condensation over moving subcooled liquid. *International Journal of Heat and Mass Transfer* **44**, 2983-2994.
[37] Scardovelli R., Zaleski S., 1999. Direct numerical simulation of free-surface and interfacial flow., 567–603.
[38] Smereka P., Sethian J. A. 2003. Level set methods for fluid interfaces, *Annual Review of Fluid Mechanics* **35,** 341-372.
[39] Streicher W., 2000. Minimising the risk of water hammer and other problems at the beginning of stagnation of solar thermal plants- a theoretical approach. *Solar Energy* **69**, 187-196.
[40] Štrubelj L., Tiselj I., 2005. Simulation Of Kelvin-Helmholtz Instability With Cfx Code. *Proceedings of the 4th international conference on transport phenomena in multiphase systems - HEAT'2005*, Gdansk, Poland.
[41] Taitel Y., Dukler A. E., 1976. Model for predicting flow regime transitions in horizontal and near horizontal gas-liquid flow. AICHE Journal 22 (1), 47-55.
[42] Thorpe, S. A. 1969. Experiments on the instability of stratified shear flows: immiscible fluids. *Journal of Fluid Mechanics*, **39**, 25–48.
[43] Tiselj, I., Černe, G., Horvat, A., Gale, J., Parzer, I., Giot, M., Seynhaeve, J. M., Kucienska, B., Lemonnier, H., 2004. WAHA3 code manual, *WAHALoads project deliverable D10*, http://www2.ijs.si/~r4www/WAHA3_manual.pdf
[44] TRAC-PF1/MOD1, 1986: An Advanced Best-Estimate Computer Program for Pressurized Water Reactor Thermal-Hydraulic Analysis, NUREG/CR-3858, L.A-10157-MS.
[45] Tsai W. T. , Yue D. K. P., 1996. Computation of nonlinear free-surface flows. *Annual Review of Fluid Mechanics*, **28**, 249-78.
[46] Unverdi O., Tryggvason G., 1992. A front-tracking method for viscous, incompressible, multi-fluid flows, Journal of Computational Physics, **100**, 25-37.
[47] Yadigaroglu G. 2005. Computational fluid dynamics for nuclear applications: from CFD to multi-scale CMFD. *Nuclear Engineering and Design* **235**, 153-164.
[48] Yao W., Coste P., Bestion D., Boucker M., 2003. Two-phase pressurized thermal shock investigations using a 3D two-fluid modeling of stratified flow with condensation. The 10th international Topical Meeting on Nuclear Reactor Thermal Hydraulics (NURETH-10).
[49] Yao Z, Hao P., Wang X., 1999. Condensation-induced water hammer analysis on the steam generator accident relief system. *Transactions of the 15th International conference on structural Mechanics in reactor technology (SMiRT-15)* J03/4.
[50] Zhang Q., Hewitt G. F., Leslie D. C., 1993, Nuclear safety code modeling of condensation in stratified flow. *Nuclear Engineering and Design* **139** (1), 1-15.